Thickness Biased on CO_2 Capture by Carbide MXenes

Ángel Morales-García*, Marc Mayans-Llorach, Francesc Viñes, Francesc Illas

Departament de Ciència de Materials i Química Física & Institut de Química Teòrica i Computacional (IQTCUB), Universitat de Barcelona. c/ Martí i Franquès 1-11, 08028 Barcelona, Spain

Abstract

The synthesis of two-dimensional transition metal carbides (MXenes) with a predefined number of atomic layers offers a possible way to tune their chemical activity. MXenes have been theoretically predicted to be able to store/release CO_2 even at high temperatures and low CO_2 partial pressures, a prediction which has been experimentally confirmed. In the present work, the influence of the number of atomic layers on CO_2 adsorption/desorption is systematically investigated by means of density functional theory (DFT) based calculations using suitable periodic models representing the (0001) surface of a series of these materials with formula $M_{n+1}C_n$ (M = Ti, Zr, Hf, V, Nb, Ta, Mo, W) and n = 1–3. The interaction of CO_2 with the MXene is always favorable with the adsorption energy decreasing as the transition metal electronic configuration goes from d^2 to d^3 and d^4, in agreement with previous work for n =1. The influence of the thickness is found to be rather small but noticeable and quite erratic. Nevertheless, the adsorption energy converges to a clear limit for sufficiently thick MXenes. Interestingly, this value is close to that corresponding to the (111) surface of bulk transition metal carbides (TMC). Indeed, the close structural similarity between the MXene(0001) and TMC(111) surfaces strongly suggests that the former provide a practical way to approach this otherwise unstable surface. The possibility to tune the CO_2 interaction based on MXenes thickness is further investigated by means of kinetic phase diagrams. These provide additional evidence that carbide MXene surfaces are promising materials CO_2 capture even at low CO_2 partial pressures and that MXene thickness can be used to fine tune this behavior.

INTRODUCTION

Two-dimensional (2D) inorganic materials exhibit a large surface-to-volume ratio, interesting physical properties, and normally high chemical activities even at room temperature. In principle, these features grant them a high capability for adsorbing gas phase molecules such as NH_3, H_2, H_2S, CH_4, CO, CO_2, N_2, NO_x or O_2.[1] Among many 2D materials, transition metal dichalcogenides (TMDs),[2-4] metals oxides,[5] group III-VI semiconductors[6] and *h*-BN sheets[7] have shown a noted activity and attracted additional interest due to the influence that the lamellar thickness has on the sensitive detection tuning. However, despite the many advantages of these materials, sensitivity, selectivity, and recovery aspects need further improvements. Interestingly, MXene materials,[8] one of the latest incorporations to the 2D family, have revealed outstanding sensitive and very high signal-to-noise ratio. These features allows one overcoming previous limitations and have triggered a high expectation in the field.[9] In particular, the as-prepared MXenes possess an hydrophilic nature and exhibit abundant highly active functional groups at the surface, so that they are able to effectively adsorb various pollutants showing outstanding adsorptive environmental applications.[10,11]

MXenes are synthetized from their layered MAX precursors;[12] a large family of ternary carbides and nitrides including solid solutions and ordered double transition metal structures.[13,14] The MAX phases are constituted by $M_{n+1}X_n$ layers of a transition metal, M, being carbides (X=C) or nitrides (X=N), interleaved with layers of an A-element (mainly a *p* block element). Chemically speaking, M–A bonds are weaker than M–X bonds, which facilitates the selective etching of A following a top-down synthesis strategy. This disassembly can be carried out by using normally aqueous hydrofluoric acid (HF),[8] although other fluorine-free,[15] or high temperature treatments syntheses have been achieved.[16] Furthermore, bottom-up synthesis methods have been utilized to fabricate high-quality 2D ultrathin α-Mo_2C crystals by using chemical vapor deposition (CVD).[17,18] It is common to denote ordered MXenes with the general $M_{n+1}X_nT_x$ (n=1–3) formula, where M and X are as defined above and T_x stands for the type of surface termination (typically OH, O, F, or H) that, depending on synthesis condition, cover the MXene surface.[19,20] Here, one must emphasize that the synthesis of termination-free, pristine MXenes ($M_{n+1}X_n$) is remarkably difficult owing to the chemical agents used for the selective etching that functionalize the surface. However, post-synthesis heat treatments combined with H_2 exposure have been recently reported providing a suitable procedure to remove the T_x species from the Ti_3C_2 surface.[21]

MXenes have potential applications in different routes of gas separation such as H_2 purification in methanol reforming process, H_2 recovery in ammonia production, and CO_2 capture for zero-emission fossil fuel power generation.[22-25] Exfoliated MXene $Ti_3C_2T_x$ nanosheets have been used as building blocks to fabricate 2D laminated membranes for selective gas separation with a H_2/CO_2 selectivity superior to the state-of-the-art membranes.[26,27] In addition, density functional theory (DFT) based calculations suggest that N_2, CO_2 and H_2O molecules can be chemisorbed on the surface of M_3C_2 MXenes.[28,29] Attending to the strength of the binding energies, carbide and nitride MXenes exhibit a prominent CO_2-philicity even triggering the molecule activation through a charge transfer towards the CO_2, thus leading to the formation of adsorbed $CO_2^{\delta-}$

species.[30,31] Therefore, MXenes have arisen as promising active substrates for carbon capture and storage (CCS) based strategies.[32] In fact, CO_2 abatement on M_2X (X = C or N) (0001) surfaces has been recently investigated by means of DFT computational approaches coupled to reaction rate theory.[33,34] These showed that MXenes can adsorb CO_2 even at low partial pressures and elevated temperatures. In addition, these materials are predicted to yield CO_2 uptakes up to ~10 mol CO_2 kg^{-1} of substrate, competitive to other nowadays-existent materials like zeolites or graphene derivates.[35,36] More recently, these theoretical predictions have been confirmed by experiments on partially bare Ti_3C_2 MXene showing a highly selectivity towards CO_2 over N_2, with uptakes of up to 12 mol CO_2 kg^{-1} for the Ti_3C_2 MXene.[21]

The previous results highlighted the large adsorptive and CCS capabilities of MXenes, and even the possible effect of the MXene stoichiometry on these properties. However, the concomitant electronic structure effect remains undisclosed, with open questions such as how far is MXenes surface activity compared to bulk transition metal carbide (TMC) surfaces. In the present work, we tackle this point by studying the effect of the MXene thickness on the CO_2 adsorption, also considering it as a factor to engineer the gas capture activity. To this end we investigate the CO_2 adsorption on a broad family of MXenes with M_2C, M_3C_2, and M_4C_3 (M = Ti, Zr, Hf, V, Nb, Ta, Mo, and W) chemical formula, comparing the results to the (001) and (111) surfaces of the related TMCs. Moreover, adsorption/desorption probabilities are studied in the framework of newly developed kinetic phase diagrams, providing estimates of partial CO_2 pressure and temperature conditions at which the MXene surfaces are suitable for the CCS strategy.

COMPUTATIONAL STRATEGY AND MODELS

To investigate the effect of MXene thickness on the CO_2 capture, we rely on first-principles periodic DFT based calculations carried out on suitable surface models. In particular, we explore $M_{n+1}C_n$ (0001) surfaces with M = Ti, Zr, Hf, V, Nb, Ta, Mo, W and n=1–3, as well as TMC (001) and (111) surfaces. The two latter introduced for comparison purposes. All DFT based calculations have been carried out using in the Vienna *Ab initio* simulation package (VASP),[37,38] employing the Perdew-Burke-Ernzerhof (PBE)[39] implementation of the generalized gradient approximation (GGA) for the exchange-correlation potential, augmented with the D3 method to account for dispersive forces.[40] The Kohn-Sham equations were solved by using an expansion of the valence electron density in a plane-wave basis set with a kinetic energy cut-off of 415 eV. The projector-augmented wave (PAW) method was included to account the interaction between the valence electron density and the atomic cores.[41] Numerical integrations in the reciprocal space werecarried out using a Monkhorst-Pack grid of 5×5×1.[42] The geometry optimizations were considered converged when forces acting on nuclei were all below 0.01 eV $Å^{-1}$. This computational setup ensures converged results up to 1 meV in the calculated adsorption energies.

It must be noted that the extended TMC (111) surfaces could be considered polar, *i.e.*, can be M- or C-terminated although the fact that these TMCs display metallic conductivity suggest that this is not an important issue. Nevertheless, the influence of this surface dipole moment on the adsorption energy has been

investigated in detail for some selected cases, comparing the results in models where such a surface dipole is present to those where it is counteracted with the standard procedure. This set of results show that the presence of the surface dipole reduces the adsorption energy by solely at most 0.05 eV, as expected. Therefore, this effect has been not further considered. The adsorption and activation of CO_2 on extended TMC (001) surfaces was previously investigated by some of us using the same computational scheme, and here included for comparison.[43]

To quantify the strength of the interaction between the CO_2 and the different MXene surfaces we rely on the adsorption energy, defined as $E_{ads} = E_{CO_2/Substrate} - (E_{Substrate} + E_{CO_2}) + \Delta E_{ZPE}$, where $E_{CO_2/Substrate}$ is the energy of CO_2 adsorbed on the substrate, $E_{Substrate}$ corresponds to the energy of the relaxed pristine MXene or TMC substrate, and E_{CO_2} stands for the energy of an isolated CO_2 molecule calculated in a symmetric box of 9×10×11 Å dimensions and using Γ-point only. The difference in the zero-point energy (ΔE_{ZPE}) of each term contribution was calculated within the harmonic approximation assuming a decoupling of the MXene phonons and the adsorbed CO_2 vibrations including frustrated rotations/translations. According to the definition of E_{ads}, the strongest interactions correspond to the most negative values.

As aforementioned, five different surfaces have been investigated so as to inspect the influence of the MXene thickness on the CO_2 adsorption energy, see Figure 1a. These include three MXene types with M_2C, M_3C_2, and M_4C_3 stoichiometries —having 3, 5, and 7 atomic layers—as well as the rocksalt TMC (001) and (111) surfaces. Note that while for these rocksalt (face-centered cubic – *fcc*) TMCs the (001) is the most stable one, as the (111) exhibits much higher cleavage energy, which indeed hampers its experimental exhibition.[44] Interestingly, the atomic structure of the $M_{n+1}C_n$(0001) surface is reminiscent to the TMC (111) one, which, as shown later on, has strong implications.

Several surface adsorption sites, accompanied by different CO_2 molecular orientations, were explored. Five sites and/or conformations (Figure 1b) emerging from these structural searches were confirmed as stable minima in at least one of the MXene (0001) and TMC (111) surfaces. The different active sites were distinguished by specifying the location of the *n* surface atoms in contact with the CO_2 molecule, adsorbed either on a surface bridge (B) site, or on a hollow, with one carbon of the second layer beneath (C) or a metal atom (M). Note that, due to the different surface atomic arrangement, the adsorption sites on the TMC (001) surfaces follow a different notation as described in an earlier work,[43,45] where it was found that the CO_2 molecule creates a C-C bond with a surface carbon atom, and the O atoms can be either bound to surface metal atoms or pointing away from the surface.[43]

RESULTS AND DISCUSSION

First the influence that MXene thickness (see Figure 1a) has over the CO_2 adsorption strength has been analyzed. Table 1 compiles the E_{ads} values for MXenes with M_2C, M_3C_2, and M_4C_3 stoichiometry classified according to the *d* series of transition metals: d^2 (Ti, Zr, and Hf), d^3 (V, Nb, and Ta), and d^4 (Mo, and W). Note that carbide Cr-derived MXenes have not been considered in the present study due to their endothermic CO_2

adsorption, as recently reported on M_2C MXenes.[33] Results in Table 1 evidence a systematic and general trend governed by the *d* series and regardless of the MXene stoichiometry. Carbide MXenes containing d^2 metals present the largest adsorption strength, below -3.0 eV, followed by those including d^3 metal MXenes with moderate adsorption energies *circa* -2.5 eV, and d^4 metal MXenes, which show the smallest E_{ads} values, yet above -1.7 eV. To ease the analysis of the influence of the thickness on the CO_2 adsorption energy, the calculated E_{ads} values *versus* the C/M ratio is represented in Figure 2, revealing a clear increase with the MXene thickness. At first sight, one could consider the thickness effect on CO_2 E_{ads} as small, although it can be significant. One can readily see that among d^2 MXenes, Ti_2C exhibits the largest adsorption energy which is 0.4 eV larger than for Ti_3C_2 and Ti_4C_3. However, decreasing along the d^2 series, one finds that the CO_2 E_{ads} for Zr_4C_3 and Hf_4C_3 becomes 0.2 and 0.1 eV larger than for the Zr_2C/Zr_3C_2 and Hf_2C/Hf_3C_2 thinner MXene counterparts, respectively. The trend, thus, is that while moving down along the d^2 series the CO_2 E_{ads} increases as the number of atomic layers in the MXenes increases. The trend in the d^3 series is, however, slightly different with V_2C featuring the strongest adsorption, predicted to be 0.2 eV larger than the corresponding values for V_3C_2 and V_4C_3. However, in the case of Nb and Ta MXenes, the largest E_{ads} values, -2.3 and -2.7 eV, correspond to Nb_3C_2 and Ta_3C_2, respectively. Therefore, when moving down along the d^3 series the adsorption strength increases from M_2C to M_3C_2 but decreases from M_3C_2 to M_4C_3 stoichiometry. Finally, the situation of the d^4 series is more homogeneous; the Mo_2C features the strongest adsorption, which is 0.3 eV larger than the value for Mo_3C_2. The cases of W-derived MXenes feature an even different trend with the estimated E_{ads} being essentially invariable with respect to the MXene thickness. This detailed description discloses that, while the MXene thickness has a clear influence on the CO_2 E_{ads}, the trends along each series are different without any clear tendency emerging from the electronic configuration of the involved transition metal. This random behavior can be tentatively attributed to the nanoscale effect emerging from the ultrasmall thickness of these materials, which still differs from those bulk limits.

To verify the above hypothesis, we compare the E_{ads} values for the explored MXenes to the corresponding values for the TMC (111) (001) surfaces, see Table 1. As already mentioned, for the rocksalt TMCs, the TMC (001) surface is the most stable one according to experimental measures and DFT based calculations.[46,47] Hence, it is not surprising to find that this surface stability is accompanied by rather low E_{ads} values well below -1.6 eV as reported in Table 1.[43] The case of the TMC (111) surfaces is especially interesting, given that the E_{ads} values are quite close to those of the M_3C_4 (0001) MXenes. This outcome is quite relevant since, for these bulk TMCs, the formation of the TMC (111) surface requires large cleavage energies, as previously reported through DFT estimates.[44,48] In fact, these estimates imply that the energy to cleave TMC (111) surfaces is at least twice that of TMC (001) surfaces. Consequently, bulk TMCs seldom exhibit these (111) surfaces. Here it is interesting to note that a comparison of the atomic structure of the MXene (0001) and TMC (111) surfaces reveals striking similarities. In fact, both exhibit the same type of atomic stacking and surface sites. Therefore, MXenes can be also though as convenient models of the otherwise highly unstable TMC (111) surfaces. As a corollary, the present work shows that MXenes provide

a promising alternative to investigate the chemistry of bulk TMC (111) surfaces. In addition, MXene (0001) surfaces have the additional advantage of a high surface-area-to-volume, which is missing in bulk TMC surfaces. This feature enables an efficient capture of gases such as CO_2 making these low dimensional materials quite attractive and promising for their usage as low-temperature gas sensor devices.[49,50] For instance, 2D V_2CT_x gas sensors are able to detect trace amounts of non-polar gases such as hydrogen and methane.[51] The predicted high performance of carbide MXenes for the adsorption of CO_2 is accompanied by a significant activation reflected in electronic changes on the CO_2 molecule and O-C-O angle, both induced by the charge transfer from the substrate, which is in the -0.80 to -2.00 *e* range directly depending on the calculated E_{ads} value,[33] being consistent with the O-C-O angle which goes from 180º in the gas phase to 111-134º when adsorbed on an MXene.

Up to here, the present results undoubtedly demonstrated that carbide MXene surfaces lead to an exothermic activation of the CO_2 molecule, which can be slightly tuned by choosing the appropriate MXene and its thickness. These results suggest, in principle, a promising workability of these 2D materials as potential substrates for CCS strategies.[32] In such a process, the CO_2 can be captured from different sources, including air, industrial sources or power plant flue gases, using either adsorption or potentially membrane gas separation technologies. In the following, the viability of carbide MXenes for such technologies is further analyzed based on adsorption and desorption rate estimates, acquired through collision and transition state theories (TST), respectively.[52] In particular, we use this approach to estimate the CO_2 partial pressures and temperatures at which the different MXene (0001) carbide surfaces are adequate, or not, for CCS. The kinetic phase diagrams for each MXene, exemplified in Figure 3 for V- and Hf-based TMC and MXenes systems, are built based on equaling the adsorption and desorption rates (r_{ads} and r_{des}) over a temperature range above 1000 K. The CCS–to–non-CCS crossover line is identified at the condition where the $r_{ads} = r_{des}$ equilibrium condition is fulfilled. Three representative operative conditions of CO_2 partial pressure (p_{CO_2}) are highlighted, including the atmospheric partial pressure of CO_2 (air), p_{CO_2} = 40 Pa;[53] a partial pressure which is a reference value for post-combustion exhaust gases (exhaust), $p_{CO_2} = 15 \cdot 10^3$ Pa;[54] and a reference value for pure CO_2 stream generation from a CCS system (desorption), $p_{CO_2} = 10^5$ Pa.[55]

Hence, Figure 3 shows the kinetic phase diagrams corresponding to the $V_{2n}C_n$ (0001) (top) and $Hf_{2n}C_n$ (bottom) MXenes including the cases of the VC(001), VC(111), HfC(001) and HfC(111) surfaces for comparison. Results in Table 1 and Figure 1 show that these particular cases are representative limiting cases of the different systems under study. The complete set of kinetic phase diagrams is supplied in the supporting information (SI). To interpret these diagrams, we first focus on the hafnium carbide systems, see bottom panel of Figure 3. In the Hf-based systems, one readily sees that HfC (001) surfaces are effective for the CCS from air up to 600 K, and above this temperature CO_2 desorbs. Here, the light blue shaded region implies temperature and p_{CO_2} conditions at which the CCS is a priori feasible, and the rest of conditions at higher temperatures and lower p_{CO_2} would not be suited for CCS —although they can be for other TMC surfaces and MXenes, and so colored, but for these other surfaces. Interestingly, for the $Hf_{2n}C_n$ (0001) and HfC (111)

surfaces the transient point is above 1000 K. Specifically, Hf_2C, Hf_3C_2, Hf_4C_3 MXenes are appropriate for CCS up to 1300, 1350, and 1400 K, respectively. Finally, the HfC(111) surface (light blue-red-green-dark blue-gray region) shows the best performance with an optimal CCS temperature of almost 1500 K. Particularly for TMCs, such high temperatures are reachable, given their refractory properties.[56] The CCS–to–non-CCS crossover lines depicted in the kinetic phase diagrams in Figure 3 are actually quite directly related to the E_{ads} values reported in Table 1 and displayed in Figure 2. This indeed explains the poor CCS performance of the VC(001) compared to the much better performance of $V_{2n}C_n$ (0001) and VC (111) surfaces, where CCS capabilities are predicted to be valid in the range of 950-1100 K for the CO_2 atmospheric partial pressure. Note also that the critical temperature at which the CCS becomes unfeasible depends on the CO_2 partial pressures, widening the temperature range even for higher CO_2 partial pressures.

The present results agree with previous studies on CO_2 uptake, *e.g.* on cleaned Ti_3C_2, with uptakes of 12 mol kg^{-1} at 373 K in agreement with the present kinetic phase diagram, see Figure S3 in the SI. Aside, recently, the CO_2 capture on $Ti_3C_2T_x$ and V_2CT_x MXenes has been experimentally detected under 0–4 MPa ($4 \cdot 10^5$ Pa) at 298 K,[25] implying the displacement of the termination species by CO_2, given the high E_{ads}, in accordance to the present findings and kinetic phase diagrams, and also why the observed desorption curves indicate that the adsorbed CO_2 cannot be released under atmospheric pressure, again in agreement with the large E_{ads} predicted for the carbide MXene (0001) surfaces, regardless the material thickness.

CONCLUSIONS

The interaction between the CO_2 molecule and $M_{n+1}C_n$ (0001) carbide MXene surfaces with n=1–3 and M=Ti, Zr, Hf, V, Nb, Ta, Mo, W has been investigated by means of first-principle periodic DFT based calculations including dispersion and ZPE contributions. Overall, for all the studied MXenes, independently of their thickness, the adsorption energies are quite large, which is already remarkable indeed, and agrees with previous predictions for the particular cases of M_2C MXenes containing three atomic layers only.[33] The present systematic study shows that the CO_2 adsorption energy is the largest for the d^2-metal containing MXene compounds, followed by d^3- and d^4-metal containing MXene ones. The influence of the MXene thickness on the CO_2 adsorption energy is rather small, yet noticeable, although without featuring a monotonous trend with the MXene thickness.

Interestingly, the comparison of CO_2 adsorption properties of the scrutinized MXenes to the corresponding values for the (111) surface of bulk transition metal carbides evidences that the latter can be seen as the limit case for the MXenes as their thickness increases. This is a very important result as the (111) surface of TMCs is very unstable and, hence, very hard to be obtained experimentally. On the other hand, this high instability confers these materials an interestingly high surface chemistry. The present results show that the carbide MXene (0001) surfaces provide a way to reach such TMC surfaces.

The obtained kinetic phase diagrams have been acquired through estimates of the adsorption and desorption rates, and allow one estimating the CO_2 partial pressure and temperature conditions where the

studied MXene compounds are suitable potential substrates for CCS technologies. The present results confirm that the carbide MXene surfaces are promising materials for capturing CO_2, with a rather small influence of the MXene thickness. For such materials the CCS–to–non-CCS crossover conditions are generally found at high temperatures and even low CO_2 partial pressures.

The present results are in good agreement with available experimental data, thus reinforcing the present general prediction and, in particular, suggest that the kinetic phase diagrams reported in this study could be considered as an initial guide for the usage of MXenes for CCS purposes. Finally, the present study strongly suggests that adsorption properties of MXenes are likely to converge fast with thickness to the values for the, otherwise hardly attainable, (111) transition metal carbide surfaces. This, however, remains to be investigated in future studies involving different types of adsorbates.

AUTHOR INFORMATION

Corresponding Author

*E-mail: angel.morales@ub.edu

Notes

The authors declare no competing financial interest.

ACKNOWLEDGMENTS

The authors acknowledge financial support from *Ministerio de Economía y Empresa* MINECO/FEDER CTQ2015-64618-R, *Ministerio de Ciencia, Innovación y Universidades* MICIUN RTI2018-095460-B-I00 and *María de Maeztu* MDM-2017-0767 grants and, in part, *Generalitat de Catalunya* 2017SGR13 and XRQTC grants. A. M.-G. thanks to MICIUN for a *Juan de la Cierva* postdoctoral research contract (IJCI-2017-31979), F. V. is thankful to *Ministerio de Economía y Competitividad* (MEC) for his *Ramón y Cajal* (RYC-2012-10129) research contract, and F. I. acknowledges additional support from the 2015 ICREA Academia Award for Excellence in University Research.

Table 1. Adsorption energies (E_{ads}) of CO_2 molecule on the studied MXene (0001) surfaces and on TMC (001) and (111) surfaces, all values given in eV. Note that E_{ads} correspond to the most favorable energies regardless the adsorption site. The C/M ratio is shown, distinguishing MXenes from bulk TMCs situations. Those E_{ads} in bold indicate the MXene thickness featuring the strongest CO_2 adsorption.

	M	**MXenes**			**TMC**	
		M_2C[a]	**M_3C_2**	**M_4C_3**	**(111)**	**(001)[b]**
C/M		**0.50**	**0.66**	**0.75**	**1.00**	
***d*²**	**Ti**	**-3.69**	-3.28	-3.37	-3.47	-0.82
	Zr	-3.16	-3.15	**-3.34**	-3.44	-1.60
	Hf	-3.36	-3.33	**-3.43**	-3.54	-1.65
***d*³**	**V**	**-2.41**	-2.19	-2.26	-2.41	-0.28
	Nb	-2.11	**-2.35**	-1.94	-2.34	-0.86
	Ta	-2.37	**-2.67**	-2.02	-2.31	-1.20
***d*⁴**	**Mo**	**-1.63**	-1.32	-1.43	-1.43	-1.20
	W	**-1.31**	**-1.31**	**-1.32**	-1.15	—

[a] Ref. 33, [b] Ref. 43

Figure 1. (a) MXenes models with M_2C, M_3C_2, and M_4C_3 stoichiometries and those of TMC (001) and (111) extended surfaces employed to investigate CO_2 adsorption. Notice the resemblance of MXene (0001) surfaces to TMC (111) ones. The (001) and (111) TMC surfaces are identified by black planes. (b) Top (bottom panel) and side (top panel) views of CO_2 adsorbed on diverse surface sites of MXene (0001) and TMC (111) surfaces. Note that only the metal layer that interacts with the CO_2 molecule is depicted in the side views. The MXene (0001) surface is depicted by dark and light blue spheres for M upper, and inner and bottom layers, respectively, whereas the inner carbon layer is represented by dark yellow spheres. The CO_2 molecule is represented by red and brown spheres, which correspond to oxygen and carbon atoms, respectively. The details about the adsorption sites on TMC (001) surface can be found in Ref. 43.

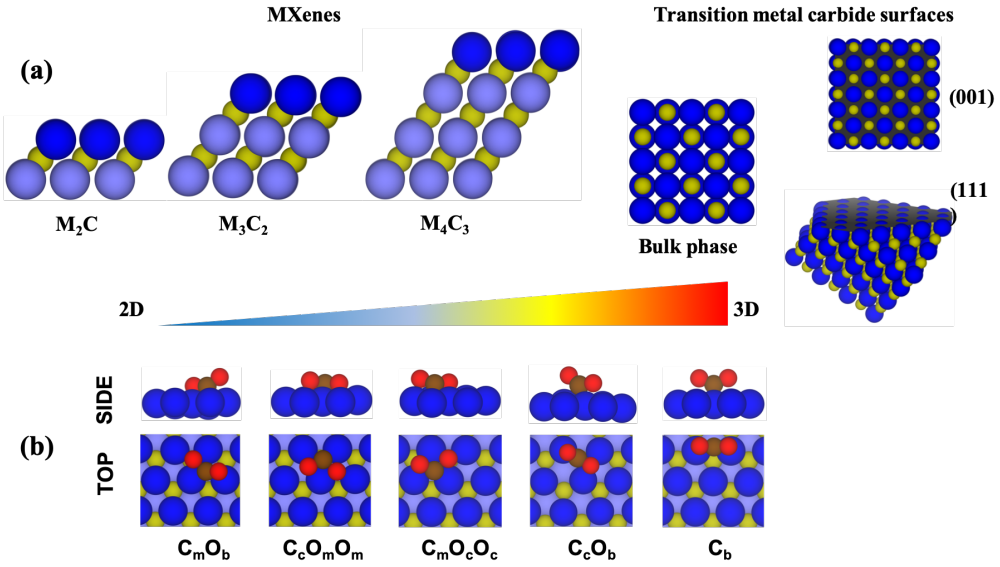

Figure 2. CO_2 adsorption energy, E_{ads}, trends along the C/M ratio of MXenes and TMC surfaces. The dash-point black lines guide the eyes to differentiate the MXenes composed by d^2, d^3, and d^4 transition metals. Values are taken from Table 1.

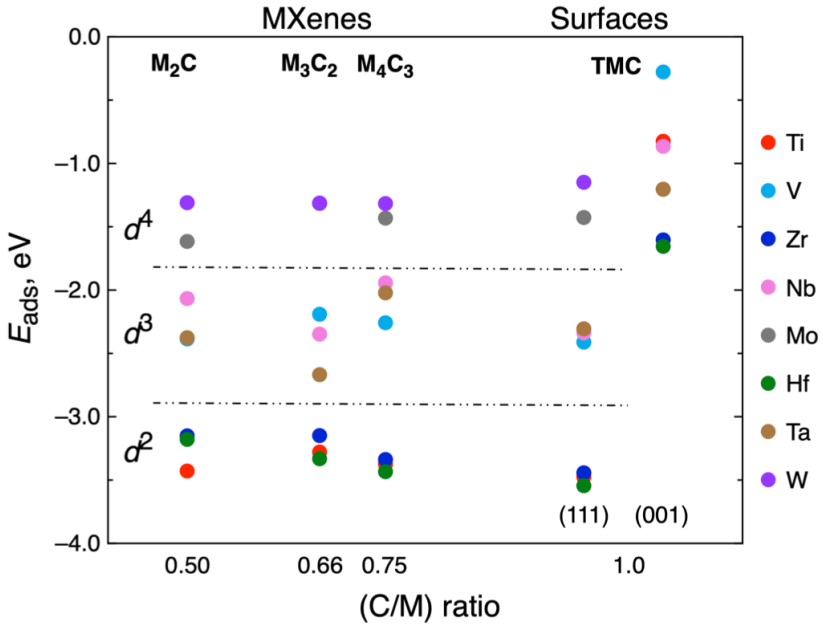

Figure 3. Kinetic phase diagrams for $V_{n+1}C_n$ (top panel) and $Hf_{n+1}C_n$ (bottom panel) MXene (0001) surfaces, along with their parent TMC (001) and (111) surfaces. White dashed dot lines stand for the atmospheric partial pressure of CO_2 (air, p_{CO_2} = 40 Pa), the CO_2 partial pressure in exhaust gases (exhaust, p_{CO_2}=15·10^3 Pa), and the CO_2 partial pressure for pure CO_2 stream generations (desorption, p_{CO_2} = 10^5 Pa).

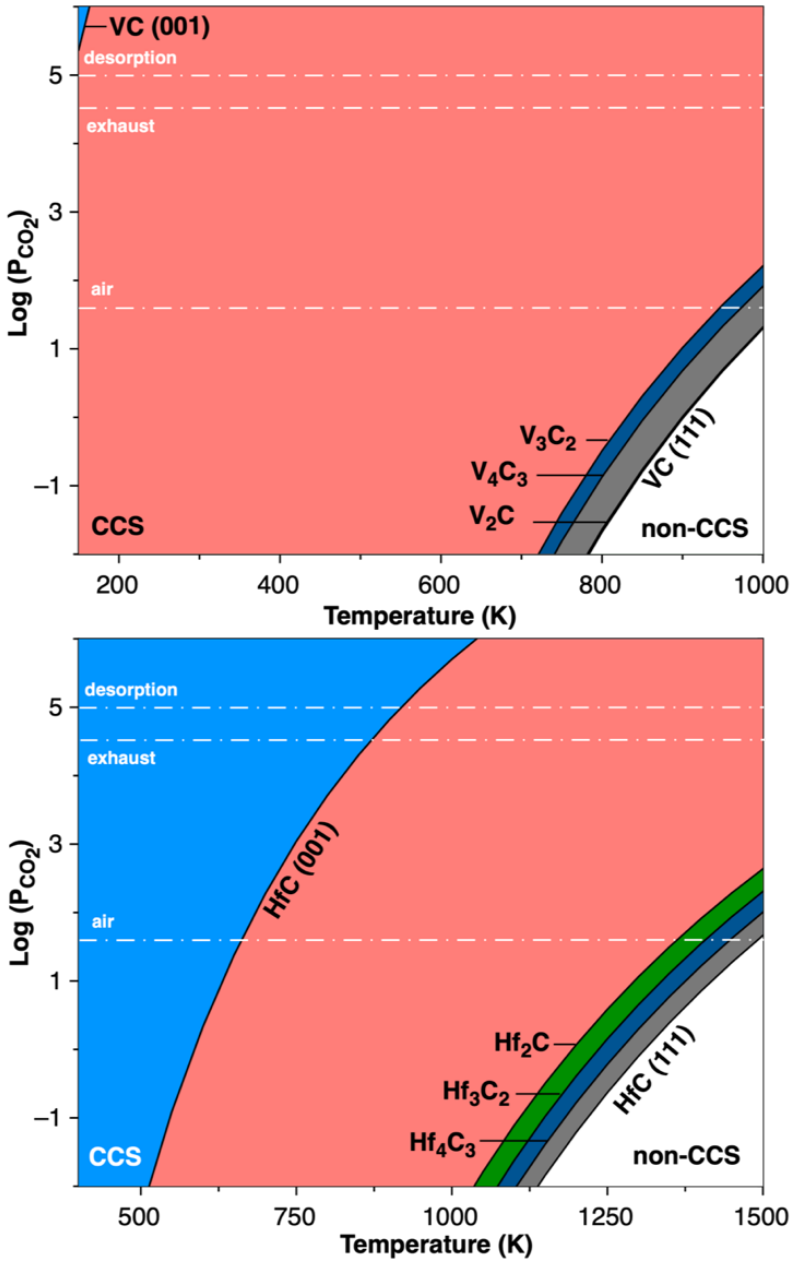

REFERENCES

(1) Yuan, W.; Shi, G. Graphene-Based Gas Sensors. *J. Mater. Chem. A* **2013**, *1*, 10078-10091.

(2) Late, D. J.; Huang, Y.-K.; Liu, B.; Acharya, J.; Shirodkar, S. N.; Luo, J.; Yan, A.; Charles, D. Waghmare, U. V.; Dravid, V. P.; Rao, C. N. R. Sensing Behavior of Atomically Thin-Layered MoS2 Transistors. *ACS Nano* **2013**, *7*, 4879-4891.

(3) Ko, K. Y.; Song, J.-G.; Kim, Y.; Choi, T.; Shin, S.; Lee, C. W.; Lee, K.; Koo, J.; Lee, H.; Kim, J.; Lee, T.; Park, J.; Kim, H. Improvement of Gas-Sensing Performance of Large-Area Tungsten Disulfide Nanosheets by Surface Functionalization. *ACS Nano* **2016**, *10*, 9287-9296.

(4) Zeng, Y.; Lin, S.; Gu, D.; Li, X. Two-Dimensional Nanomaterials for Gas Sensing Applications: The Role of Theoretical Calculations. *Nanomaterials* **2018**, *8*, 851 (1-16).

(5) Uppuluri, R.; Gupta, A. S.; Rosas, A. S.; Mallouk T. E. Soft Chemistry of Ion-Exchangeable Layered Metal Oxides. *Chem. Soc. Rev.* **2018**, *47*, 2401-2430.

(6) Ou, J. Z.; Ge, W.; Carey, B.; Daeneke, T.; Rotbart, A.; Shan, W.; Wang, Y.; Fu, Z.; Chrimes, A. F.; Wlodarski, W.; Russo, S. P.; Li, Y. X.; Kalantar-Zadeh, K. Physisorption-Based Charge Transfer in Two-Dimensional SnS_2 Selective and Reversible NO_2 Gas Sensing. *ACS Nano* **2015,** *9*, 10313-10323.

(7) Ayari, T.; Bishop, C.; Jordan, M. B.; Sundaram, S.; Li, X.; Alam, S.; ElGmili, Y.; Patriarche, G.; Voss, P. L.; Salvestrini, J. P.; Ougazzaden, A. Gas Sensors Boosted by Two-Dimensional *h*-BN Enabled Transfer on Thin Substrate Foils: Towards Wearable and Portable Applications. *Sci. Rep.* **2017**, *7*, 15212 (1-8).

(8) Naguib, M.; Kurtoglu, M.; Presser, V.; Lu, J.; Niu, J.; Heon, M.; Hultman, L.; Gogotsi, Y.; Barsoum, M. W. Two-Dimensional Nanocrystals Produced by Exfoliation of Ti3AlC2. *Adv. Mater.* **2011**, *23*, 4248-4253.

(9) Kim, S. J.; Koh, H.-J.; Ren, C. E.; Kwon, O.; Maleski, K.; Cho, S.-Y.; Anasori, B.; Kim, C.-K.; Choi, Y.-K.; Kim, J.; Gogotsi, Y.; Jung, H.-T. Metallic Ti3C2Tx MXene Gas Sensors with Ultrahigh Signal-to-Noise Ratio. *ACS Nano* **2018**, *12*, 986-993.

(10) Zhang, Y.; Wang, L.; Zhang, N.; Zhou, Z. Adsorptive Environmental Applications of MXene Nanomaterials: A Review. *RSC Adv.* **2018**, *8*, 19895-19905.

(11) Zhang, Y.; Zhang, N.; Ge, C. First-Principles Studies of Adsorption Remediation of Water and Air Pollutants Using Two-Dimensional MXene Materials. *Materials* **2018**, *11*, 2281 (1-12).

(12) Sokol, M.; Natu, V.; Kota, S.; Barsoum, M. W. On the Chemical Diversity of the MAX Phases. *Trends Chem.* **2019**, *1*, 210-223.

(13) Barsoum, M. W.; Radovic, M. Elastic and Mechanical Properties of the MAX Phases. *Annu. Rev. Mater. Res.* **2011**, *41*, 195-227.

(14) Eklund, P.; Beckers, M.; Jansson, U.; Högberg, H.; Hultman, L. The Mn+1AXn Phases: Materials Science and Thin-Film Processing. *Thin Solid Films* **2010**, *518*, 1851-1878.

(15) Li, T.; Yao, L.; Liu, Q.; Gu, J.; Luo, R.; Li, J.; Yan, X.; Wang, W.; Liu, P.; Chen, B.; Zhang, W.; Abbas, W.; Naz, R.; Zhang, D. Fluorine-Free Synthesis of High-Purity $Ti_3C_2T_x$ (T=OH, O) via Alkali Treatment. *Angew. Chem. Int. Ed.* **2018**, *57*, 6115-6119.

(16) Urbankowski, P.; Anasori, B.; Makeryan, T.; Er, D.; Kota, S.; Walsh, P. L.; Zhao, M.; Shenoy, V. B.; Barsoum, M. W.; Gogotsi, Y. Synthesis of Two-Dimensional Titanium Nitride Ti_4N_3 (MXene). *Nanoscale* **2016**, *8*, 11385-11391.

(17) Gogotsi, Y. Chemical Vapour Deposition: Transition Metal Carbides Go 2D. *Nat. Mater.* **2015**, *14*, 1079-1080.

(18) Xu, C.; Wang, L.; Liu, Z.; Chen, L.; Guo, J.; Kang, N.; Ma, X. L.; Cheng, H. M.; Ren. W. Large-Area High-Quality 2D Ultrathin Mo_2C Superconducting Crystals. *Nat. Mater.* **2015**, *14*, 1135-1141.

(19) Naguib, M.; Mochalin, V. N.; Barsoum, M. W.; Gogotsi, Y. MXenes: A New Family of Two-Dimensional Materials. *Adv. Mater.* **2014**, *26*, 992-1004.

(20) Hart, J. L.; Hantanasirisakul, K.; Lang, A. C.; Anasori, B.; Pinto, D.; Pivak, Y.; van Omme, J. T.; May, S. J.; Gogotsi, Y.; Taheri, M. L. Control of MXenes´ Electronic Properties Through Termination and Intercalation. *Nat. Commun.* **2019**, *10*, 522.

(21) Persson, I.; Halim, J.; Lind, H.; Hansen, T. W.; Wagner, J. B.; Näslund, L.-Å.; Darakchieva, V.; Palisaitis, J.; Rosen, J.; Persson, P. O. Å. 2D Transition Metal Carbides (MXenes) for Carbon Capture. *Adv. Mater.* **2019**, *31*, 1805472 (1-5).

(22) Ding, L.; Wei, Y.; Li, L.; Zhang, T.; Wang, H.; Xue, J.; Ding, L.-X.; Wang, S.; Caro, J.; Gogotsi, Y. MXene Molecular Sieving Membranes for Highly Efficient Gas Separation. *Nat. Commun.* **2018**, *9*, 155 (1-7).

(23) Shen, J.; Liu, G.; Ji, Y.; Liu, Q.; Cheng, L.; Guan, K.; Zhang, M.; Liu, G.; Xiong, J.; Yang, J.; Jin, W. 2D MXene Nanofilms with Tunable Gas Transport Channels. *Adv. Func. Mater.* **2018**, *28*, 1801511 (1-13).

(24) Li, L.; Zhang, T.; Duan, Y.; Wei, Y.; Dong, C.; Ding, L.; Qiao, Z.; Wang, H. Selective Gas Diffusion in Two-Dimensional MXene Lamellar Membranes: Insights from Molecular Dynamics Simulations. *J. Mater. Chem. A* **2018**, *6*, 11734-11742.

(25) Wang, B.; Zhou, A.; Liu, F.; Cao, J.; Wang, L.; Hu, Q. Carbon Dioxide Adsorption of Two-Dimensional Carbide MXenes. *J. Adv. Ceram.* **2018**, *7*, 237-245.

(26) Li, H.; Haas-Santo, K.; Schygulla, U.; Dittmeyer, R. Inorganic Microporous Membranes for H_2 and CO_2 Separation–Review of Experimental and Modeling Progress. *Chem. Eng. Sci.* **2015**, *127*, 401-417.

(27) Liu, G.; Shen, J.; Ji, Y.; Liu, Q.; Liu, G.; Yang, J.; Jin, W. Two-Dimensional Ti_2CT_x MXene Membranes with Integrated and Ordered Nanochannels for Efficient Solvent Dehydration. *J. Mater. Chem. A* **2019**, *7*, 12095-12104.

(28) Azofra, L. M.; Li, N.; MacFarlane, D. R.; Sun, C. Promising Prospects for 2D d^2–d^4 M_3C_2 Transition Metal Carbides (MXenes) in N_2 Capture and Conversion into Ammonia. *Energy Environ. Sci.* **2016**, *9*, 2545-2549.

(29) Li, N.; Chen, X.; Ong, W.-J.; MacFarlane, D. R.; Zhao, X.; Cheetham, A. K.; Sun, C. Understanding of Electrochemical Mechanisms for CO_2 Capture and Conversion into Hydrocarbon Fuels in Transition-Metal Carbides (MXenes). *ACS Nano* **2017**, *11*, 10825-10833.

(30) Viñes, F.; Borodin, A.; Höfft, O.; Kempter, V.; Illas, F. The Interaction of CO_2 with Sodium promoted W(011). *Phys. Chem. Chem. Phys.* **2005**, *7*, 3866-3873.

(31) Freund, H.-J.; Roberts, M. W. Surface Chemistry of Carbon Dioxide. *Surf. Sci. Rep.* **1996**, *25*, 225-273.

(32) Leung, D. Y. C.; Caramanna, G. An Overview of Current Status of Carbon Dioxide Capture and Storage Technologies. *Renewable Sustainable Energy Rev.* **2014**, *39*, 426-443.

(33) Morales-García, Á.; Fernández-Fernández, A.; Viñes, F.; Illas, F. CO_2 Abatement Using Two-Dimensional MXene Carbides. *J. Mater. Chem. A* **2018**, *6*, 3381-3385.

(34) Morales-Salvador, R.; Morales-García, Á.; Viñes, F.; Illas, F. Two-Dimensional Nitrides as Highly Efficient Potential Candidates for CO_2 Capture and Activation. *Phys. Chem. Chem. Phys.* **2018**, *20*, 17117-17124.

(35) Chen, C.; Park, D.-W.; Ahn, W.-S. CO_2 Capture Using Zeolite 13X Prepared from Bentonite. *Appl. Surf. Sci.* **2014**, *292*, 63-67.

(36) Chowdhury, S.; Balasubramanian, R. Three-Dimensional Graphene-Based Porous Adsorbents for Postcombustion CO_2 Capture. *Ind. Eng. Chem. Res.* **2016**, *55*, 7906-7916.

(37) Kresse, G.; Furthmüller, J. Efficient Iterative Schemes for *ab initio* Total-Energy Calculations Using a Plane-Wave Basis set. *Phys. Rev. B* **1996**, *54*, 11169-11186.

(38) Kresse, G.; Furthmüller, J. Efficiency of *ab-initio* Total Energy Calculations for Metals and Semiconductors Using a Plane-Wave Basis set. *Comput. Mater. Sci.* **1996**, *6*, 15-50.

(39) Perdew, J. P.; Burke, K.; Ernzerhof, M. Generalized Gradient Approximation Made Simple. *Phys. Rev. Lett.* **1996**, *77*, 3865-3868.

(40) Grimme, S.; Antony, J.; Ehrlich, S.; Krieg, H. A Consistent and Accurate *ab initio* Parametrization of Density Functional Dispersion Correction (DFT-D) for the 94 Elements H-Pu. *J. Chem. Phys.* **2010**, *132*, 154104 (1-19).

(41) Blöchl, P. E. Projector Augmented-Wave Method. *Phys. Rev. B* **1994**, *50*, 17953-17979.

(42) Monkhorst, H. J.; Pack, J. D. Special Points for Brillouin-Zone Integrations. *Phys. Rev. B* **1976**, *13*, 5188-5192.

(43) Kunkel, C.; Viñes, C.; Illas, F. Transition Metal Carbides as Novel Materials for CO_2 Capture, Storage, and Activation. *Energy Environ. Sci.* **2016**, *9*, 141-144.

(44) Vojvodic, A.; Ruberto, C.; Lundqvist, B. I. Atomic and Molecular Adsorption on Transition-Metal Carbide (111) Surfaces from Density-Functional Theory: A trend Study of Surface Electronic Factors. *J. Phys. Condens. Matter.* **2010**, *22*, 375504.

(45) Posada-Pérez, S.; Viñes, F.; Ramírez, P. J.; Vidal, A. B.; Rodríguez, J. A.; Illas, F. The Bending Machine: CO_2 Activation and Hydrogenation on δ-MoC(001) and β-Mo_2C(001) Surfaces. *Phys. Chem. Chem. Phys.* **2014**, *16*, 14912-14921.

(46) Zaima, S.; Shibata, Y.; Adachi, H.; Oshima, C.; Otani, S.; Aono, M.; Ishizawa, Y. Atomic Chemical Composition and Reactivity of the TiC(111) Surface. *Surf. Sci.* **1985**, *157*, 380-392.

(47) Viñes, F.; Sousa, C.; Liu, P.; Rodriguez, J. A.; Illas, F. A Systematic Density Functional Theory Study of the Electronic Structure of Bulk and (001) Surface of Transition-Metals Carbides. *J. Chem. Phys.* **2005**, *122*, 174709.

(48) do Santos Politi, J. R.; Viñes, F.; Rodríguez, J. A.; Illas F. Atomic and Electronic Structure of Molybdenum Carbide Phases: Bulk and Low Miller-Index Surfaces. *Phys. Chem. Chem. Phys.* **2013**, *15*, 12617-12625.

(49) Tang, X.; Du, A.; Kou, L. Gas Sensing and Capturing Based on Two-Dimensional Layered Materials: Overview from Theoretical Perspective. *WIREs Comput. Sci.* **2018**, *8*, e1361.

(50) Lee, E.; VahidMohammadi, A.; Prorok, B. C.; Yoon, Y. S.; Beidaghi, M.; Kim, D.-J. Room temperature Gas Sensing of Two-Dimensional Titanium Carbide (MXene). *ACS Appl. Mater. Interfaces* **2017**, *9*, 37184-37190.

(51) Lee, E.; VahidMohammadi, A.; Yoon, Y. S.; Beidaghi, M.; Kim, D.-J. Two-Dimensional Vanadium Carbide MXenes for Gas Sensors with Ultrahigh Sensitivity Nonpolar Gases. *ACS Sens.* **2019**, *4*, 1603-1611.

(52) Reuter, K. *Modelling and Simulation of Heterogeneous Catalytic Reactions*, Wiley-VCH Verlag GmbH & Co. KGaA: New York, NY, **2011**.

(53) Takahashi, T.; Sutherland, S. C. *Global Ocean Surface Water Partial Pressure of CO_2 Database: Measurements Performed During 1957-2017*. National Centers for Environmental Information. National Oceanic and Atmospheric Administration: Silver Spring, MD, **2018**.

(54) D´Alessandro, D. M.; Smit, B.; Long, J. R. Carbon Dioxide Capture: Prospects for New Materials. *Angew. Chem., Int. Ed.* **2010**, *49*, 6058-6082.

(55) Boot-Handford, M. E.; Abanades, J. C.; Anthony, E. J.; Blunt, M. J.; Brandani, S.; MacDowell, N.; Frenández, J. R.; Ferrari, M.-C.; Gross, R.; Hallett, J. P.; Haszeldine, R. S.; Heptonstall, P.; Lyngfelt, A.; Makuch, Z.; Mangano, E.; Porter, R. T. J.; Pourkashanian, M.; Rochelle, G. T.; Shah, N.; Yao, J. G.; Fenneli, P. S. Carbon Capture and Storage Update. *Energy Environ. Sci.* **2014**, *7*, 130-189.

(56) Hwu, H. H.; Chen, J. G. Surface Chemistry of Transition Metal Carbides. *Chem. Rev.* **2005**, *105*, 185-212.

TOC